

# Automatic Framework for Spectral-Spatial Classification based on Supervised Feature Extraction and Morphological Attribute Profiles

Pedram Ghamisi, *Student Member, IEEE*, Jón Atli Benediktsson, *Fellow, IEEE*, Gabriele Cavallaro, *Student Member, IEEE*, Antonio Plaza, *Senior Member, IEEE*

**Abstract**—Supervised classification plays a key role in terms of accurate analysis of hyperspectral images. Many applications can greatly benefit from the wealth of spectral and spatial information provided by these kind of data, including land-use and land-cover mapping. Conventional classifiers treat hyperspectral images as a list of spectral measurements and do not consider spatial dependencies of the adjacent pixels. To overcome these limitations, classifiers need to use both spectral and spatial information. In this paper, a framework for automatic spectral-spatial classification of hyperspectral images is proposed. In order to extract the spatial information, Extended Multi-Attribute Profiles (EMAPs) are taken into account. In addition, in order to reduce the redundancy of features and address the so-called curse of dimensionality, different supervised feature extraction techniques are considered. The final classification map is provided by using a Random Forest classifier. The proposed automatic framework is tested on two widely used hyperspectral data sets; Pavia University and Indian Pines. Experimental results confirm that the proposed framework automatically provides accurate classification maps in acceptable CPU processing times.

**Index Terms**—Hyperspectral Image Analysis, Extended Multi-Attribute Profile (EMAP), Random Forest Classification, Supervised Feature Extraction.

## I. INTRODUCTION

**H**YPERSPECTRAL imaging instruments are now able to capture hundreds of spectral channels from the same area on the surface of the Earth. By providing very fine spectral resolution with hundreds of (narrow) bands, accurate discrimination of different materials is possible. In parallel, thanks to recent advances in hyperspectral technology, the spatial resolution of the sensors is becoming also finer, which allows for a detailed characterization of spatial structures in the scene.

Supervised classification techniques play a key role in the analysis of hyperspectral images and a wide variety of applications can be handled by successful classifiers in the literature [1], including: land-use and land-cover mapping, crop monitoring, forest applications, urban development, mapping, tracking and risk management.

In the spectral domain, each spectral channel is considered as one dimension. By increasing the dimensionality in the spectral domain, theoretical and practical problems arise. Some of these problems are related to the curse of dimensionality, which is related to the unbalance between the (high) dimensionality of the input data and the (often limited) number of training samples used in the supervised classification

process [2]. In [3], Landgrebe shows that too many spectral bands can be undesirable from the standpoint of expected classification accuracy. In other words, when the number of spectral bands (dimensionality) increases, with a constant number of training samples, the accuracy of the statistics estimation decreases. The aforementioned issue demonstrates that there is an optimal number of bands and that (given an available set of training samples) more features do not necessarily lead to better results. Therefore, feature reduction techniques may lead to better classification accuracies [4].

Conventional classifiers treat hyperspectral images as a list of spectral measurements with no particular arrangement [5], and do not consider spatial dependencies of adjacent pixels. In other words, conventional techniques classify images only based on their spectral information alone. Therefore, these approaches discard information associated with the spatial correlations among distinct pixels in the image. In order to address the aforementioned issue, the consideration of both spectral and spatial information has been widely explored in the literature [6]. In addition, spatial information can provide additional information related to the shape and size of different structures, which generally leads to better classification accuracies and classification maps.

Two strategies are commonly used in order to characterize spatial information; crisp neighborhood system and adaptive neighborhood system. While the first one mostly considers spatial and contextual dependencies in a predefined neighborhood system, the latter is more flexible and it is not confined to a given neighborhood system. One way for extracting spatial information with crisp neighborhood is to consider Markov Random Field (MRF) modeling. MRF is a family of probabilistic models that can be described as a 2-D stochastic process over discrete pixel lattices [7]. There is extensive literature on the use of MRFs in classification, such as [8, 9]. However, the main disadvantages of considering a set of crisp neighbors are that i) the standard neighborhood system may not contain enough samples, which decreases the effectiveness of the classifier (in particular, when the input data set is of high resolution and the neighboring pixels are highly correlated [6]); and ii) a larger neighborhood system leads to computationally intractable problems [6]. In order to address the aforementioned issues, adaptive neighborhood systems can be taken into consideration. A possible way to develop adaptive neighborhood systems is to use different types of segmentation methods. Image segmentation is a procedure

which can be used to modify the accuracy of classification maps [10]. To make such an approach effective, an accurate segmentation of the image is needed [11]. Several works have previously explored the extraction of spatial information using segmentation techniques (e.g., [12], [13] and [14]). Another set of methods which can extract spatial information by using adaptive neighborhood systems relies on morphological filters. Pesaresi and Benediktsson [15] used morphological transformations to build a so-called Morphological Profile (MP). In [16], the MP was used to handle hyperspectral images and named Extended MP (EMP) in this context. Attribute Profiles (APs) constitute another extension of the concept of MP, and provide a multilevel characterization of an image by the sequential application of morphological attribute filters which model different specifications of the structural information contained in the scene [17]. APs provide a powerful tool to increase the discrimination of different classes [17], [18]. However, there are two main difficulties associated with the concept of EMAP, including: i) how to establish which attributes lead to a better discrimination for different classes, and ii) how to determine which values should be considered in order to initialize each AP.

In this paper, a new fully automatic approach is proposed for accurate classification of hyperspectral images. Although the presented framework can be also used for classification of multispectral images with coarser spectral resolution, it is used here for spectral-spatial classification of hyperspectral images. In order to extract the spatial information, Extended Multi-Attribute Profiles (EMAP) [17] are automatically generated by the proposed framework. In order to reduce the redundancy of the data and address the so-called curse of dimensionality, different supervised feature extraction techniques are also included in the proposed framework. The final classification map is provided by a Random Forest (RF) classifier [19] [20]. In order to handle high dimensional data, RF and SVM have been widely considered as the most powerful classifiers since they are robust when handling high dimensional data with a limited number of training samples. Both the SVM and RF classifiers are comparable in terms of classification accuracies and have been widely used for the purpose of hyperspectral image classification. However, while both methods are shown to be effective classifiers for non-linear classification problems, SVM requires a computationally demanding parameter tuning process in order to achieve optimal results, whereas RF does not require such a tuning process. In this sense, RF is faster than SVM. In this paper, our main objective is obtaining good classification accuracies in an acceptable CPU processing time. In addition, several studies such as [21] have reported that Hughes phenomenon [2] is more evident when the number of dimensions is high and the data are classified by SVM instead of RF. The proposed approach is tested using two well-known data sets collected by the Reflective Optics Spectrographic Imaging System (ROSIS) over the city of Pavia, Italy, and by the Airborne Visible Infra-Red Imaging Spectrometer (AVIRIS) over the Indian Pines region in northwestern Indiana. The experimental results confirm that the presented framework is able to classify hyperspectral images efficiently both in terms of classification accuracies and CPU processing time. It

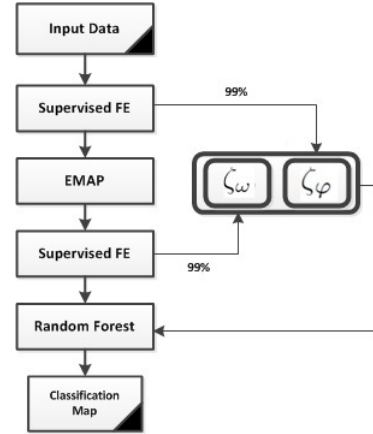


Fig. 1. A flowchart of the proposed framework.

should be noted that the proposed approach is fully automatic and there is no need to initialize any parameters empirically. The main contribution of this paper compared to other works on EMAP is that, in most of previous works, the EMAP is built using an unsupervised feature extraction approach such as Principal Component Analysis (PCA), Independent Component Analysis (ICA) and Kernel PCA, while in this work we explore the use of supervised feature extraction for this purpose. Another main difference is concerned with the automatic nature of our approach in the sense that, in previous works, threshold values for making EMAP needed to be initialized manually while, in the present framework, a general range of parameter values is used to make the parameter selection automatic. Another important difference is that, in most previous works, the outcome of the attribute profile is directly used for classification, while in our framework we use a second feature extraction strategy prior to classification. As will be shown by the present contribution, the results of the second feature extraction step are used for classification purposes by our proposed framework, with concatenating features of both feature extraction steps in one vector and then performing the classification step.

This remainder of the paper is organized as follows: the proposed framework is discussed in Section II. Section III is devoted to validating the framework via extensive experimental results. Section IV outlines the main conclusions and provides hints at plausible future research lines.

## II. FRAMEWORK

In the proposed framework, supervised Feature Extraction (FE) is first performed on the input data and the first features with cumulative eigenvalues above 99% are retained. In the case of Discriminant Analysis Feature Extraction (DAFE), the criterion is related to the size of the eigenvalues of the scatter matrices. In the case of Decision Boundary Feature Extraction (DBFE), it is related to the size of the eigenvalues of the decision boundary feature matrix. Let us consider  $\zeta_\varphi$  as the output of this step. Then, EMAPs are built on the first few features and the resulting features are concatenated into one stacked vector. In order to reduce the redundancy

of the stacked vector, a supervised feature extraction step is performed once again. Let  $\zeta_\omega$  be the output of this step. The final classification map is provided by performing RF classification on the stacked vector;  $\zeta = [\zeta_\varphi, \zeta_\omega]^T$ . Fig. 1 illustrates the proposed framework by a flowchart. In the following, the individual parts of the proposed framework will be discussed in detail.

#### A. Feature Extraction (FE)

FE consists of finding a set of vectors that represent an observation while reducing its dimensionality. Feature extraction techniques can be grouped into two categories; unsupervised approaches and supervised approaches where the former is used for the purpose of data representation and the latter is considered for overcoming the Hughes phenomena and reducing the redundancy of data in order to improve classification accuracies. PCA is an example of unsupervised feature extraction. PCA does not find optimum feature sets in the sense of class discrimination and discards class specific information. Therefore, for image classification, supervised feature extraction may lead to higher classification accuracies. From one point of view, supervised feature extraction techniques can be split into two categories; parametric and non-parametric. The main disadvantages of non-parametric feature extraction techniques is that they do not have an assumption on the underlying density functions in the data. Therefore, feature extraction for non-parametric classifiers is often not feasible or very time consuming. On the contrary, although the computation cost of non-parametric classifiers is often much larger than that of parametric classifiers, there are some cases where the use of non-parametric feature extraction is desirable. For example, if the underlying densities are unknown or problems involve complex densities, which cannot be approximated by a common parametric density functions, the use of a non-parametric classifier is important [22]. In this work, two approaches are considered for supervised FE: DAFE and DBFE. Below, the considered supervised feature extraction techniques are briefly explained.

1) *DAFE*: This approach is widely used for dimension reduction in classification problems [23]. Since, DAFE uses the mean vector and the covariance matrix of each class, it is considered as supervised feature extraction. In DAFE, within-class, between-class and mixture scatter matrices are usually considered as the criteria for class separability. DAFE is fast and works well when the distribution of the data is normal. Otherwise, the performance of DAFE may not be satisfactory. Another problem associated with this method is that if the difference in the class-mean vectors is small, the feature chosen may not be reliable. Similarity, if one class-mean vector is very different from others, its class will dominate the others in the computation of the between-class covariance matrix [24]. As a consequence, the feature extraction process may be ineffective. In addition, DAFE performs the computations with full dimensionality, which requires a large number of training samples in order to

accurately estimate parameters. A main shortcoming of DAFE is that DAFE is not full rank and its rank is at maximum  $L-1$  where  $L$  is the number of classes. Let us assume that the rank of the within-class scatter matrix is  $u$ ; in this case only  $\min(L-1, u)$  features are selected by using DAFE. Since the complexity of the data in real scenarios could be quite high, using only  $L-1$  features may not be enough to fully characterize the data.

2) *DBFE*: This method was proposed in [25] where it was shown that both discriminantly informative and redundant features can be extracted from the decision boundary between two classes. The features are extracted from the Decision Boundary Feature Matrix (DBFM). In order to obtain the same classification accuracy as in the original space, keeping the eigenvectors of the decision boundary feature matrix corresponding to nonzero eigenvalues is crucial. The performance of this method does not deteriorate even when there is no difference in the mean vectors or covariance matrices. It should be noticed that this approach does not rely on the number of classes in the same way as DAFE. The efficiency of DBFE is highly dependent on the quality and number of training samples, which is not desirable. Another shortcoming of DBFE is that it can be computationally intensive.

#### B. EMAP

Mathematical Morphology [26–29], is a well established framework which provides operators able to high-quality spatial features. Fundamental mathematical morphology operators, such as Erosion and Dilation (and their combinations: opening and closing) examine the geometrical structures in the image by matching them to small patterns, called Structuring Elements. Depending on the shape and size of the Structuring Element, undesirable effects can occur in the filtered image; in particular, geometrical characteristics of the structures can be distorted or completely lost. In this work, morphological operators are considered which perform transformations by reconstruction, a class of connected filters [30]. Specifically, they act on connected components, i.e., flat regions of a gray scale image, which are either completely removed or preserved according to their interaction with the Structuring Element adopted by the transformation.

1) *Attribute filters based on tree representation*: Attribute Filters [31] are flexible operators that can perform a simplification of a grayscale image driven by an arbitrary measure which can be related to characteristics of regions in the scene such as the scale, shape, contrast etc. Improvements in terms of capability in modeling the spatial information are achievable since these operators are not based on fixed Structuring Elements and the image transformation is only computed by merging its connected components. The idea is to extract different types of information, represented by the attributes, from different flat regions, i.e., parts of the scene with the same gray levels. Attribute Filters are efficiently implemented with an equivalent representation of the image as a tree [32].

In particular, a thresholding operation of all the mapped values present in the image  $f$ , results in upper and lower level sets which are connected components (i.e., flat zones) that can be grouped in the following sets:

- $\mathcal{U}(f) = \{X : X \in \mathcal{CC}([f \geq \lambda]), \lambda \in \mathbb{Z}\}$ ,
- $\mathcal{L}(f) = \{X : X \in \mathcal{CC}([f < \lambda]), \lambda \in \mathbb{Z}\}$ ,

with  $\mathcal{CC}(f)$  being the connected components of the generic image  $f$ . There is an inclusion relationship [33] between the connected components extracted by both the upper or lower level sets (belonging to  $\mathcal{U}(f)$  or  $\mathcal{L}(f)$ , respectively). This property allows for the association of a node in the tree to each connected component and thus represent the image as a hierarchical structure: the max-tree and min-tree [32] structures represent, respectively, the components in  $\mathcal{U}(f)$  and  $\mathcal{L}(f)$  with their inclusion relations by the thresholding operations. Attribute filters are shape preserving, since they never introduce new edges in an image [32], and operate on regions according to the result of a binary predicate  $P$ . In particular, the filtering criteria usually determine whether the value of an attribute  $\alpha$  of a given connected component  $CC$  verifies a predicate:  $P = \alpha(CC) \geq \lambda$  with  $\{\alpha(CC), \lambda\} \in \mathbb{R}$  or  $\mathbb{Z}$ , where  $\lambda$  is a threshold value. When attribute filters are applied to the tree representation of the image, the operator leads to a pruning of the tree by removing the nodes whose associated regions do not fulfill  $P$ . Two different filtering approaches have been proposed: pruning the tree by removing whole branches, and pruning by not removing all the branches [34]. Attributes can be purely geometric (e.g., area, length of the perimeter, moment of inertia) or textural (e.g., standard deviation, entropy). A very detailed characterization of features is usually obtained.

2) *Attribute Profiles*: The spatial features can be derived in different ways such as with Gray-Level Co-occurrence Matrix (GLCM), Differential Morphology Profiles (DMPs) or Urban Complexity Index (UCI) [35]. Here we propose to use EMAPs instead of GLCM, DMPs and UCI. The use of EMAPs based on mathematical morphology concepts exhibit some desirable features in the context of hyperspectral image classification. Specifically, they offer a very flexible approach since they can perform the processing based on many different types of attributes. In fact, the attributes can be of any type. For example, they can be purely geometric, or related to the spectral values of the pixels, or on different characteristics. Furthermore, an efficient implementation based on tree representation has been used. In summary, EMAP offer a different strategy to include spatial information when compared to GLCM or UCI.

The spatial information belonging to different features present in very high resolution data can be efficiently exploited by considering a multilevel approach based on morphological Attribute Filters. In particular, APs define a general set of profiles which take advantage of the flexibility of the Attribute Filters in order to better investigate the scene. According to the type of the criteria (increasing, non-increasing), Attribute Profiles are defined differently. In the case of increasing attributes, the attribute profile is a sequence of attribute openings

and closings which include morphological opening and closing profiles by reconstruction [36]. On the other hand, when dealing with increasingness criteria, attribute thinning and thickening over a multi-level approach is applied. The result is the obtained attribute thinning and thickening profiles, which perform a multi-level analysis of the image based on attributes (represented by ordered criteria) not necessary related to the scale of the structures of the image.

APs can be therefore regarded as more effective filters than Morphological profiles; this is because the latter perform a partial characterization of the objects in the scene as a consequence of the fact that Structuring Elements are intrinsically unsuitable to describe features related to the graylevel characteristic of the region. Another considerable advantage is that attribute profiles are computed according to an effective implementation based on max-tree and min-tree representations, which lead to a reduction of the computational load when compared with conventional profiles built with operators by reconstruction.

3) *Extended Attribute Profiles*: Since hyperspectral sensors collect information in several spectral bands, EAPs which are based on morphological attribute filters are adopted in order to perform the analysis of hyperspectral high resolution images. The extension to multi-valued images is not a trivial task; morphological operators compute their function in a different domain which becomes a subset of the multivariate domain where the ordering of the mapped vector values is not defined anymore. The EAPs rely on the application of the APs to hyperspectral data and they are simply defined as [36]:

$$EAP = \{AP(PC_1), AP(PC_2), \dots, AP(PC_c)\}, \quad (1)$$

where PC name denotes a principal component obtained after applying principal component analysis (PCA) [37]. As mentioned before, PCA does not find optimum feature sets in the sense of class discrimination and discards class specific information. Therefore, for image classification, supervised feature extraction leads to higher classification accuracies since such approaches provide optimal features with respect to class specific information. The EAP includes in its definition the extended morphological profile since the operators by reconstruction can be viewed as a particular set of morphological attribute. Since the modeling of spatial features is performed by attribute filters, this approach leads to a great flexibility, and the computation of the filters on the max-tree structure reduces the computational complexity with respect to EMP since the tree is built once for each principal component and filtered multiple times, according to the required number of levels.

4) *Extended Multi-Attribute Profiles*: Attribute Profiles extract efficiently spatial features by considering different attributes; for this reason, EMAPs merges different EAPs in a single data structure [36]:

$$EMAP = \{EAP_{a_1}, EAP'_{a_2}, \dots, EAP'_{a_m}\}. \quad (2)$$

Since the dimensionality of the features is increased, the EMAP has much greater capabilities in extracting spatial information than a single EAP but, at the same time, the computational cost of processing these features is slightly higher since the max-tree and min-tree are computed only once for each PC and they are filtered with different attributes at different levels.

5) *Automatic framework*: Now an automatic framework is introduced in order to solve issues such as the automatic selection of the attributes that lead to a best possible discrimination between the classes, or the automatic identification of the most appropriate values to initialize each AP. Fig. 2 shows the general idea of the automatic framework for the construction of EMAPs. While the APs can be constructed by using a wide variety of attributes, in the automatic framework only the area and standard deviation attributes are used, since the aforementioned attributes can be adjusted in an automatic way and are well-related to the object hierarchy in the images. The standard deviation is adjusted with respect to the mean of the individual features, since the standard deviation shows dispersion from the mean [21]. Therefore,  $\lambda_s$  is initialized so as to cover a reasonable amount of deviation in the individual feature, which is mathematically given by

$$\lambda_s(Fe_i) = \frac{\mu_i}{100} \{\sigma_{min}, \sigma_{min} + \delta_s, \sigma_{min} + 2\delta_s, \dots, \sigma_{max}\}, \quad (3)$$

where  $Fe_i$  denotes the  $i$ th feature obtained by a supervised FE.  $\mu_i$  is the mean of the  $i$ -th feature and  $\sigma_{min}$ ,  $\sigma_{max}$  and  $\delta_s$  are 2.5, 27.5 and 2.5 percent, respectively, which leads to 11 thinning and 11 thickening operations. It should be noticed that the above-mentioned parameters have been tested on other well-known data sets with different spatial resolution in [18] and results confirm that these parameters are data set distribution independent and can provide excellent results in terms of classification accuracies.

With regard the adjustment of  $\lambda_a$  for the area attribute, the resolution of the image should be taken into account in order to construct the EAP [18]. The automatic construction of the attribute area is accomplished by the following expression:

$$\lambda_a(Fe_i) = \frac{1000}{v} \{a_{min}, a_{min} + \delta_a, a_{min} + 2\delta_a, \dots, a_{max}\}, \quad (4)$$

where  $a_{min}$  and  $a_{max}$  are initialized by 1 and 14, respectively, with a stepsize increase of  $\delta_a$  equal to 1. The EAP for the area attribute includes 14 thinning and 14 thickening operations for each feature. Each level is provided in square meters by considering the resolution of the image  $v$  in meters. Each profile covers structures in the range of 1000 to 14000  $m^2$ , which might be a reasonable range of sizes for different structures in both urban and rural cases in remote sensing images [18]. However, different ranges can be considered for different applications.

Regarding (3) and (4), the used parameters have been tested on other well-known data sets with different spatial resolutions in [18] and results confirm that these parameters are data set distribution independent and can provide excellent results in terms of classification accuracies. In other words, those

parameters do not need to be tuned for different data sets with different spatial resolutions. In the introduced framework, one only needs to establish a range of parameter values in order to automatically obtain a classification result with high accuracy for different data sets. It turns out that the used parameter ranges have been tested on other well-known data sets with different spatial resolutions, such as the ones described in [18], and the obtained results confirm that these parameters are data set independent. In other words, those parameter ranges can be fixed for different data sets with different spatial resolution. In [38], it was shown that the automatic scheme with only two attributes (area and standard deviation) can provide results comparable with a manual scheme with four attributes in terms of classification accuracy and CPU processing time.

### C. Fusion of extracted features via vector stacking

As indicated in Fig. 1, the input data are transformed by a supervised FE and only the first few features are used in order to reduce redundancy in the data while keeping most of the data variance. Then, the EMAP is computed by using only the first effective features that correspond to 99% of the eigenvalues.

Let  $\zeta_\varphi$  be the set of features retained. Then, MAP is performed on each feature of  $\zeta_\varphi$  and the output features are concatenated into one stacked vector. In order to address the so-called curse of dimensionality and reduce the redundancy of the stacked vector, a supervised feature extraction step is performed once again. Let  $\zeta_\omega$  be the output of this step consisting of the features with cumulative eigenvalues above 99%. The final classification map is achieved by performing RF classification on the stacked vector;  $\zeta = [\zeta_\varphi, \zeta_\omega]^T$ .

### D. Random Forest (RF)

RF was first introduced in [19]. It is an ensemble method for classification and regression. Ensemble classifiers get their name from the fact that several classifiers are trained and their individual results are then combined through a voting process. For the classification of an object from an input vector, the input vector is run down each tree in the forest. Each tree provides a unit vote for a particular class and the forest chooses the classification having the most votes. Based on [20], the computational complexity of the RF algorithm is  $cT\sqrt{MN}\log(N)$  where  $c$  is a constant,  $T$  denotes the number of trees in the forest,  $M$  is regarded as the number of variables and  $N$  is the number of samples in the data set. It is easy to infer that RF is not computationally intensive but demands a considerable amount of memory, since it is necessary to store an  $N \times T$  matrix in the process. RF has several advantages, such as the capacity to provide good classification accuracies, and to handle many variables. Another advantage of the RF classifier is that it is insensitive to noise in the training samples. In addition, RF provides an unbiased estimate of the test set error as trees are added to the ensemble, with almost no sensitivity to overfitting issues.

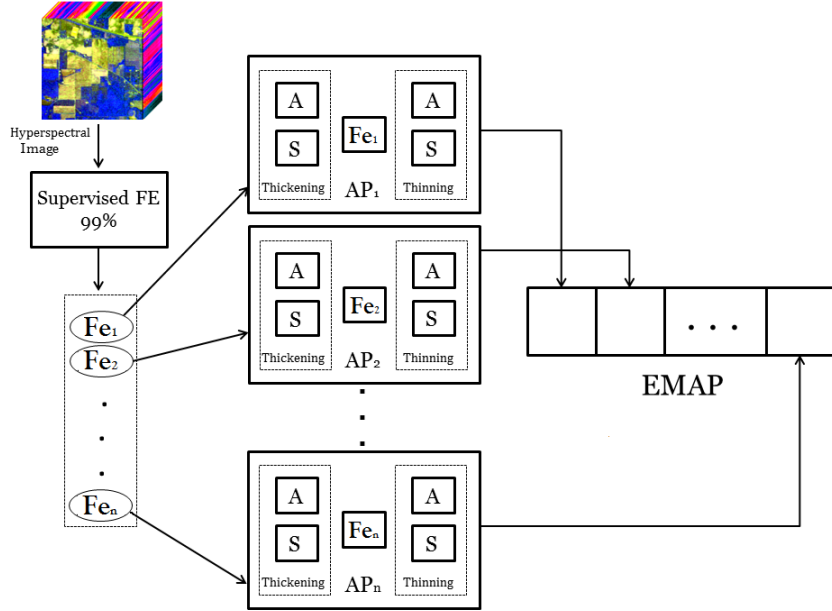


Fig. 2. Automatic Framework for the construction of EMAPs. First, a supervised Feature Extraction (FE) step is performed on the input data and the first features with cumulative eigenvalues above 99% are kept. Then, Extended Morphological Attribute Profiles (EMAPs) are built for the first few features and the output features are concatenated into one stacked vector.

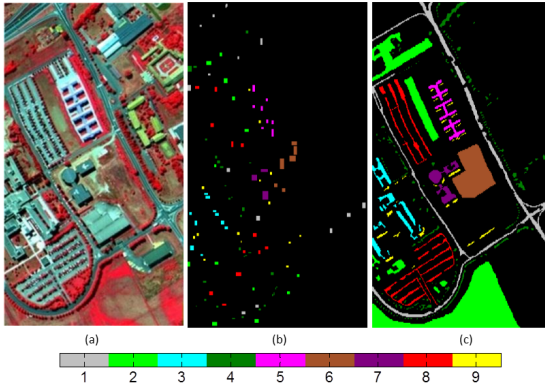


Fig. 3. The ROSIS-03 Pavia University data set. a) False color image; b) training samples, c) test samples, each color represents a specific information class. The information classes are listed in Table I.

### III. EXPERIMENTAL RESULTS

#### A. Data Description

Two hyperspectral data sets were used in experiments. They are described below.

1) *Pavia University*: The first test case is a hyperspectral data set captured on the city of Pavia, Italy by the ROSIS-03 (Reflective Optics Spectrographic Imaging System) airborne instrument. The ROSIS-03 sensor has 115 data channels with a spectral coverage ranging from 0.43 to 0.86  $\mu\text{m}$ . The data have been corrected atmospherically, but not geometrically. The spatial resolution is 1.3 m per pixel. The data set covers the Engineering School at the University of Pavia and consists of different classes including: trees, asphalt, bitumen, gravel, metal sheet, shadow, bricks, meadow and soil. In our experiments, 12 noisy data channels were eliminated and 103 data

channels used for processing. The original data set comprises  $640 \times 340$  pixels. Fig. 3(a) shows a false color composite of the Pavia University while Fig. 3(b) shows a fixed training set that will be used for training purposes in this paper. Fig. 3(c) shows the available reference data for the scene. The number of available test and training samples are listed in Table I.

2) *Indian Pines data*: The second data set used in experiments is the well-known data set captured on Indian Pines (NW Indiana) in 1992 comprising 16 classes (see Fig. 4), mostly related to different land covers. The data set consists of  $145 \times 145$  pixels with spatial resolution of 20 m/pixel. In this work, 200 data channels are used, i.e., after the removal of the spectral bands affected by atmospheric absorption. The number of training and test samples are displayed in Table II.

It should be noted that, in addition to selecting widely used data sets in the hyperspectral imaging community, we have used exactly the same training and test samples that have been considered in most works related to spectral-spatial classification of hyperspectral images. Some of the works which have considered exactly the same training and test samples are those in references [9, 39, 40]. In other words, we not only used the same number of training and test samples adopted by other state-of-the-art methods, but also these samples have exactly the same spatial locations in the data. This way of using the training and test samples makes this work fully comparable with other spectral and spatial classification techniques reported in the literature. In order to keep consistency with previous results, each method was run only once since we have not used different training and test samples, but instead used exactly the same samples as adopted in previous studies.

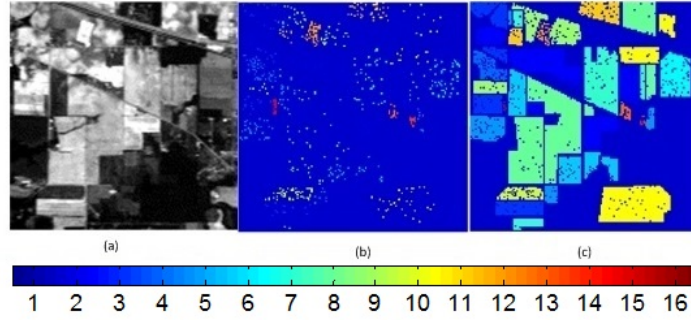


Fig. 4. The AVIRIS Indian Pines data set. a) Spectral band number 27 ( $\lambda = 646.72nm$ ); b) training samples, c) test samples, where each color represents a specific information class. The information classes are listed in Table II.

TABLE I

PAVIA UNIVERSITY: NUMBER OF TRAINING AND TEST SAMPLES ALONG WITH CLASSIFICATION ACCURACIES FOR THE RAW SPECTRAL DATA IN PERCENTAGE. THE NUMBER OF FEATURES IS GIVEN IN THE PARENTHESES

Number	Class Name	Number of Samples		Raw (103)
		Training	Test	
1	Asphalt	548	6631	80.8
2	Meadows	540	18649	56.1
3	Gravel	392	2099	53.5
4	Trees	524	3064	98.7
5	Metal Sheets	256	1345	99.1
6	Soil	532	5029	78.1
7	Bitumen	375	1330	84.3
8	Bricks	514	3682	91.0
9	Shadows	231	947	98.3
Kappa	-	-	-	0.6511
OA	-	-	-	71.64
AA	-	-	-	82.25

TABLE II

INDIAN PINES: NUMBER OF TRAINING AND TEST SAMPLES ALONG WITH CLASSIFICATION ACCURACIES FOR THE RAW SPECTRAL DATA IN PERCENTAGE. THE NUMBER OF FEATURES IS GIVEN IN THE PARENTHESES

Number	Class Name	Number of Samples		Raw (200)
		Training	Test	
1	Corn-notill	50	1384	57.5
2	Corn-mintill	50	784	58.6
3	Corn	50	184	85.8
4	Grass-pasture	50	447	85.6
5	Grass-trees	50	697	79.9
6	Hay-windrowed	50	439	94.7
7	Soybean-notill	50	918	78.5
8	Soybean-mintill	50	2418	58.8
9	Soybean-clean	50	564	62.9
10	Wheat	50	162	96.3
11	Woods	50	1244	88.5
12	Bldg-Grass-Tree-Drives	50	330	57.5
13	Stone-Steel-Towers	50	45	93.3
14	Alfalfa	15	39	53.8
15	Grass-pasture-mowed	15	11	81.8
16	Oats	15	5	100
Kappa	-	-	-	0.6642
OA	-	-	-	70.24
AA	-	-	-	76.98

### B. Experimental Setting

In experiments the input image is transformed by a supervised FE and the first features with cumulative eigenvalues above 99% are retained, since they are expected to contain most of the variance in the original data sets. In the proposed framework there is a second FE step which is conducted using the same criterion. For simplicity, the names of the different classifiers will be referred hereinafter as follows:

- *Raw*: When the input data is classified by RF.
- *Spec*: When only spectral information resulting from the first Supervised FE is classified by RF.
- *AP*: When the selected features are used in order to produce the EMAP and classified by the RF.
- *n<sub>m</sub>*: When a Supervised FE is performed for the second time and the output is classified by the RF. We have decided to use the name *n<sub>m</sub>* in this case, where *n* FE approach means that the input data set first is transformed by *n* FE approach and the EMAP is then transformed by *m* FE approach. As an example, *DB\_DA* means that the raw data were transformed by DBFE and the EMAP by DAFE.
- $\zeta_{DA}$ : Stacked vector consisting all features resulting from the first and second Supervised FE. The suffix *DA* refers to the second FE technique.
- $\zeta_{DB}$ : Stacked vector consisting of all features resulting from the first and second Supervised FE. The suffix *DB* refers to the second FE technique.

In the following, the number of features for *Spec* indicates the number of features with cumulative eigenvalues of more than 99% after performing DAFE or DBFE on the raw data. For example, it can be seen from Table III that 6 features are kept for *Spec*. It means that, first, the input data is transformed by DAFE and the first features with cumulative eigenvalues of more than 99% percent were kept (6 features). These 6 features are used as a baseline for constructing the EMAP. Then, 14 thinning and 14 thickening are produced for the area attribute and 11 thinning and 11 thickening are produced for the standard deviation attribute. Therefore, each feature was used to produce 50 attributes and, by considering the feature itself in that vector, we have 51 features for each feature obtained by DAFE ( $6 \times 51 = 306$  features for *AP*). Then, the second FE was performed and the first features with cumulative eigenvalues of more than 99% percent were kept.

In this way for Table III,  $DA\_DA$  and  $DA\_DB$  consist of 8 and 24 features, respectively.  $\zeta_{DA}$  is the combination of Spec and  $DA\_DA$  ( $6 + 8 = 14$ ) and  $\zeta_{DB}$  is the combination of Spec and  $DA\_DB$  ( $6 + 24 = 30$ ).

The way we calculate the CPU processing of each method, is listed below:

- *Spec*: CPU processing time of the first FE plus the CPU processing time of the corresponding RF classification,
- *AP*: CPU processing time of the first FE plus the CPU processing time of producing EMAP plus the CPU processing time of the corresponding RF classification,
- *n<sub>m</sub>*: CPU processing time of the first FE plus the CPU processing time of producing EMAP plus the CPU processing time of the second FE plus the CPU processing time of the corresponding RF classification,
- $\zeta_{DA\text{or}DB}$ : CPU processing time of the first FE plus the CPU processing time of producing EMAP plus the CPU processing time of the second FE plus the CPU processing time of corresponding the RF classification.

The following measures are used in order to evaluate the performance of different classification methods.

1) *Average Accuracy (AA)*: This metric shows the average value of the class classification accuracy.

2) *Overall Accuracy (OA)*: This metric refers to the number of samples which are classified correctly divided by the number of test samples.

3) *Kappa Coefficient*: This metric provides information regarding the agreement corrected by the level of agreement that could be expected due to chance alone.

5) *CPU Processing Time*: This metric shows the speed of different algorithms. It should be noted that, since in all algorithms (except Spectral), EMAP is carried out, the CPU processing time of this step is discarded from all methods. Hence, the CPU processing time is only provided for AP, AP+Spectral, DAFE and NWFE. All methods were implemented in MATLAB on a computer having Intel(R) Pentium(R) 4 CPU 3.20 GHz and 4GB of memory.

### C. Experimental Results

1) *Pavia University*: Table III gives information related to the classification accuracies of different methods after applying DAFE, with the corresponding CPU processing times listed in Table IV. As it can be observed from Tables I and III, the spectral classification with only 6 features improves the OA of the Raw, data with 103 bands by 8 percent. Also, the class accuracies of Meadows and Gravel classes can be improved. Specifically, many samples of Meadows are misclassified as belonging to Soil. Moreover, many samples of Gravel are misclassified as belonging to Asphalts and Bricks.

As can be seen from Table III,  $\zeta_{DB}$  (consisting of 30 features) outperforms other methods significantly.  $\zeta_{DB}$  improves the OA of Spectral, AP,  $DA\_DA$ ,  $DA\_DB$  and  $\zeta_{DA}$  by 18, 2.5, 11, 6 and 12 percent, respectively.

As it was already observed for the AVIRIS Indian Pines data set, AP achieves the best OA after  $\zeta_{DB}$  since AP can model spatial dependencies of different objects by considering an adaptive neighborhood system. As can be seen from Table V,

the OA of Spectral with 29 features improves the OA of Raw (with 103 bands) by 8 percent. Another observation is that AP,  $DB\_DA$ ,  $\zeta_{DA}$  and  $\zeta_{DB}$  provide good performance. However,  $DB\_DA$  with only 7 features provides the best results in terms of classification accuracies and CPU processing time.

By comparing the results reported on Tables III and V, it is easy to infer that DBFE works better than DAFE. The main reason behind this may be closely related to the fact that DAFE is not full rank (its rank is at most equal to  $L-1$  where  $L$  is the number of classes). Sometimes, the aforementioned number of features is not enough in order to discriminate between different classes of interest. However, DAFE is faster than DBFE. This fact can be also observed in Tables IV and VI. Based on our experimental results, the proposed framework improves all methods in terms of classification accuracies for the Pavia University data set. For example, the proposed method improves the classification accuracy of the classification technique proposed in [39] by almost 11 percent. Based on the results reported in [41], the proposed method improves the OA of the previous method with PCA by almost 21 percent and ICA by 3.5 percent. These are quite important achievements from the viewpoint of classification accuracy (in this regard, our framework provides some of the best classification results ever reported in the literature for the considered scene). The main disadvantage of the proposed method is the fact that the final result is dependent on the second FE and it is difficult to anticipate which one of  $\zeta_{DA}$  or  $\zeta_{DB}$  works better. The investigation of these aspects will be a subject for our future research efforts.

2) *Indian Pines*: The low spatial resolution of this data set adds more complexity, since it leads to the presence of highly mixed pixels (which are mainly due to the early growth cycle of most of the agricultural features in the scene). In this case, the classification results may be degraded by the presence of mixed pixels in the scene. In addition, the significant differences in the number of pixels in the reference data for different classes make the classification task even more complicated.

In these data, there is a high confusion between classes Soybean-mintill and corn-notill which degrades the class accuracies of both of them. By comparing Tables VII and II, it is easy to infer that, by performing DAFE on the input data and choosing the first features with cumulative eigenvalues above 99%, OA is reduced from 70.24% (Raw) to 65.47% (Spectral). This reveals that of only 13 features are not sufficient to discriminate between different classes, as compared to hundreds of spectral bands from the input data. As it can be seen from Table VII, AP improves the overall accuracy of Raw in more than 25%. The main reason behind this significant improvement is that AP not only considers the spectral information but also can model the spatial information contained in the input data. The best classification accuracies in Table VII are achieved by the proposed method;  $\zeta_{DA}$ , which improves the overall accuracy of Spectral, AP,  $DA\_DA$ ,  $DA\_DB$ ,  $\zeta_{DB}$  by almost 28, 2, 5, 8 and 9 percents, respectively. It should be noted that the new method can discriminate different classes by considering only 26 features. Moreover, the CPU processing time of the

TABLE III  
PAVIA UNIVERSITY: CLASSIFICATION ACCURACIES OBTAINED BY DIFFERENT METHODS FOR THE ROSIS PAVIA UNIVERSITY SCENE AFTER APPLYING DAFE. THE NUMBER OF FEATURES USED FOR CLASSIFICATION PURPOSES IS REPORTED IN THE PARENTHESES.

Number	Class Name	Spec (6)	AP (306)	DA_DA (8)	DA_DB (24)	$\zeta_{DA}$ (14)	$\zeta_{DB}$ (30)
1	Asphalt	82.9	98.0	98.2	97.1	<b>98.3</b>	97.0
2	Meadows	71.4	92.6	70.1	82.5	69.0	<b>96.5</b>
3	Gravel	69.5	81.0	<b>93.4</b>	89.7	91.6	86.4
4	Trees	92.2	97.8	<b>99.5</b>	99.3	<b>99.5</b>	<b>99.5</b>
5	Metal Sheets	99.9	99.8	99.9	99.8	<b>100</b>	99.8
6	Soil	87.8	98.6	99.8	<b>99.9</b>	99.7	<b>99.9</b>
7	Bitumen	84.5	<b>100</b>	99.7	<b>100</b>	99.7	99.8
8	Bricks	85.1	96.1	<b>99.4</b>	99.3	<b>99.4</b>	<b>99.4</b>
9	Shadows	<b>97.7</b>	94.5	92.5	91.0	92.4	91.5
Kappa	-	0.7426	0.9317	0.8258	0.8862	0.8187	<b>0.9619</b>
OA	-	79.63	94.77	86.13	91.13	85.54	<b>97.11</b>
AA	-	85.71	95.41	94.75	95.42	94.43	<b>96.68</b>

TABLE IV  
PAVIA UNIVERSITY: CPU PROCESSING TIME (IN SECONDS) OF DIFFERENT METHODS AFTER APPLYING DAFE.

Spec	AP	DA_DA	DA_DB	$\zeta_{DA}$	$\zeta_{DB}$
7	131	51	161	48	165

TABLE V  
PAVIA UNIVERSITY: CLASSIFICATION ACCURACIES OBTAINED BY DIFFERENT METHODS FOR THE ROSIS PAVIA UNIVERSITY SCENE SCENE AFTER APPLYING DBFE. THE NUMBER OF FEATURES USED FOR CLASSIFICATION PURPOSES IS REPORTED IN THE PARENTHESES.

Number	Class Name	Spec (29)	AP (1479)	DB_DA (7)	DB_DB (30)	$\zeta_{DA}$ (36)	$\zeta_{DB}$ (59)
1	Asphalt	85.0	<b>98.1</b>	97.8	97.3	97.6	96.7
2	Meadows	68.0	94.4	<b>97.4</b>	88.8	96.9	95.8
3	Gravel	69.4	98.0	97.2	74.7	<b>98.3</b>	87.0
4	Trees	95.2	87.3	98.3	95.2	98.5	<b>99.3</b>
5	Metal Sheets	99.8	99.6	99.5	<b>99.9</b>	<b>99.9</b>	99.8
6	Soil	93.6	<b>100</b>	99.9	99.4	<b>100</b>	99.9
7	Bitumen	86.1	<b>100</b>	99.6	99.7	99.5	99.9
8	Bricks	87.3	98.1	99.2	98.9	99.3	<b>99.4</b>
9	Shadows	<b>97.5</b>	97.1	94.0	95.9	95.7	91.8
Kappa	-	0.7441	0.9481	<b>0.9746</b>	0.9078	0.9732	0.9576
OA	-	79.56	96.04	<b>98.07</b>	92.91	97.97	96.78
AA	-	86.91	96.98	98.15	94.47	<b>98.46</b>	96.67

TABLE VI  
PAVIA UNIVERSITY: CPU PROCESSING TIME (IN SECONDS) OF DIFFERENT METHODS AFTER APPLYING DBFE.

Spec	AP	DB_DA	DB_DB	$\zeta_{DA}$	$\zeta_{DB}$
36	478	201	803	833	827

proposed method is acceptable and takes only 13 seconds to classify the input data set in the considered computing environment.

After  $\zeta_{DA}$ , AP exhibits the best performance among other techniques in terms of classification accuracies. This confirms that the consideration of spatial information has a significant influence on the discrimination of different classes. By including a second FE step, although classification accuracy for some classes such as class 3 and 4 are improved, the overall accuracy of AP is reduced from 91.13% to 88.47% ( $DA\_DA$ ) and 85.53% ( $DA\_DB$ ).

Table IX gives information related to the classification accuracies of different methods after DBFE. The

corresponding CPU processing times are listed on Table X. By comparing Tables IX and II, one can infer that the OA of the Raw classification decreases when DBFE is performed. Again, the proposed method outperforms other techniques with acceptable CPU processing time (45 seconds) in this particular case.

On the other hand, it is also important to emphasize AP exhibits an acceptable performance in terms of classification accuracies when compared to other classifiers (its performance is only slightly lower than  $\zeta_{DA}$ ). AP provides 720 features. This reveals that RF is a robust classifier when dealing with very high dimensional data. Also, it is worth mentioning that  $\zeta_{DA}$  provides the best performance overall, and improves the

TABLE VII

INDIAN PINES: CLASSIFICATION ACCURACIES OBTAINED BY DIFFERENT METHODS FOR THE AVIRIS INDIAN PINES SCENE AFTER APPLYING DAFE. THE NUMBER OF FEATURES USED FOR CLASSIFICATION PURPOSES IS REPORTED IN THE PARENTHESES.

Number	Class Name	Spec (13)	AP (663)	DA_DA (13)	DA_DB (45)	$\zeta_{DA}$ (26)	$\zeta_{DB}$ (58)
1	Corn-notil	54.3	82.7	82.8	76.1	<b>88.5</b>	76.2
2	Corn-mintill	52.8	<b>96.0</b>	95.5	90.0	95.1	88.2
3	Corn	67.9	92.9	<b>99.4</b>	96.7	98.9	95.1
4	Grass-pasture	89.9	93.7	<b>95.7</b>	94.4	94.6	94.6
5	Grass-trees	87.9	96.1	<b>97.5</b>	95.9	97.1	95.4
6	Hay-windrowed	97.0	<b>99.7</b>	98.6	99.3	98.6	99.3
7	Soybean-notill	63.8	<b>91.6</b>	81.0	87.0	86.6	83.5
8	Soybean-mintill	44.8	85.1	76.7	73.4	<b>91.3</b>	73.0
9	Soybean-clean	64.3	87.7	<b>89.8</b>	89.3	89.7	86.7
10	Wheat	98.1	99.3	99.3	<b>100</b>	99.3	<b>100</b>
11	Woods	85.2	99.3	<b>99.9</b>	91.8	99.4	93.8
12	Bldg-Grass-Tree-Drives	80.9	99.0	<b>99.3</b>	98.7	<b>99.3</b>	97.2
13	Stone-Steel-Towers	93.3	<b>100</b>	<b>100</b>	<b>100</b>	<b>100</b>	<b>100</b>
14	Alfalfa	56.4	<b>97.4</b>	94.8	<b>97.4</b>	94.8	<b>97.4</b>
15	Grass-pasture-mowed	<b>100</b>	<b>100</b>	<b>100</b>	90.9	<b>100</b>	<b>100</b>
16	Oats	80.0	<b>100</b>	<b>100</b>	<b>100</b>	<b>100</b>	<b>100</b>
Kappa	-	0.6118	0.8987	0.8683	0.8359	<b>0.9227</b>	0.8295
OA	-	65.47	91.13	88.47	85.53	<b>93.27</b>	84.99
AA	-	76.07	95.07	94.44	92.59	<b>95.86</b>	92.56

TABLE VIII

INDIAN PINES: CPU PROCESSING TIME (IN SECONDS) OF DIFFERENT METHODS AFTER APPLYING DAFE.

Spec	AP	DA_DA	DA_DB	$\zeta_{DA}$	$\zeta_{DB}$
2	17	13	64	13	65

TABLE IX

INDIAN PINES: CLASSIFICATION ACCURACIES OBTAINED BY DIFFERENT METHODS FOR THE AVIRIS INDIAN PINES SCENE AFTER APPLYING DBFE. THE NUMBER OF FEATURES USED FOR CLASSIFICATION PURPOSES IS REPORTED IN THE PARENTHESES.

Number	Class Name	Spec (16)	AP (816)	DB_DA (13)	DB_DB (43)	$\zeta_{DA}$ (29)	$\zeta_{DB}$ (59)
1	Corn-notil	51.4	79.9	71.6	75.2	<b>86.2</b>	73.7
2	Corn-mintill	56.8	96.4	96.5	90.0	<b>96.6</b>	90.4
3	Corn	72.8	88.5	<b>94.0</b>	<b>94.0</b>	<b>94.0</b>	<b>94.0</b>
4	Grass-pasture	85.2	93.5	<b>95.5</b>	93.7	95.0	93.2
5	Grass-trees	87.9	<b>99.0</b>	95.9	98.4	94.8	98.5
6	Hay-windrowed	94.3	<b>99.3</b>	99.0	99.0	99.0	99.0
7	Soybean-notill	63.6	<b>87.2</b>	78.1	80.0	86.8	77.8
8	Soybean-mintill	46.9	82.0	75.2	73.8	<b>85.9</b>	70.3
9	Soybean-clean	65.4	84.9	<b>87.2</b>	78.1	84.9	77.6
10	Wheat	99.3	<b>100</b>	98.7	<b>100</b>	<b>100</b>	<b>100</b>
11	Woods	81.1	<b>99.6</b>	99.5	94.6	99.4	93.1
12	Bldg-Grass-Tree-Drives	75.4	98.7	<b>99.7</b>	99.3	<b>99.7</b>	98.4
13	Stone-Steel-Towers	91.1	<b>100</b>	<b>100</b>	<b>100</b>	<b>100</b>	<b>100</b>
14	Alfalfa	69.2	<b>97.4</b>	<b>97.4</b>	<b>97.4</b>	<b>97.4</b>	<b>97.4</b>
15	Grass-pasture-mowed	81.8	<b>100</b>	<b>100</b>	<b>100</b>	<b>100</b>	<b>100</b>
16	Oats	40.0	<b>100</b>	<b>100</b>	80.0	<b>100</b>	80.0
Kappa	-	0.6058	0.8808	0.8388	0.8254	<b>0.9001</b>	0.8083
OA	-	64.99	89.56	85.90	84.64	<b>91.27</b>	83.11
AA	-	72.67	94.18	93.05	90.88	<b>95.01</b>	90.25

TABLE X

INDIAN PINES: CPU PROCESSING TIME (IN SECONDS) OF DIFFERENT METHODS AFTER APPLYING DBFE.

Spec	AP	DB_DA	DB_DB	$\zeta_{DA}$	$\zeta_{DB}$
26	45	44	132	45	133

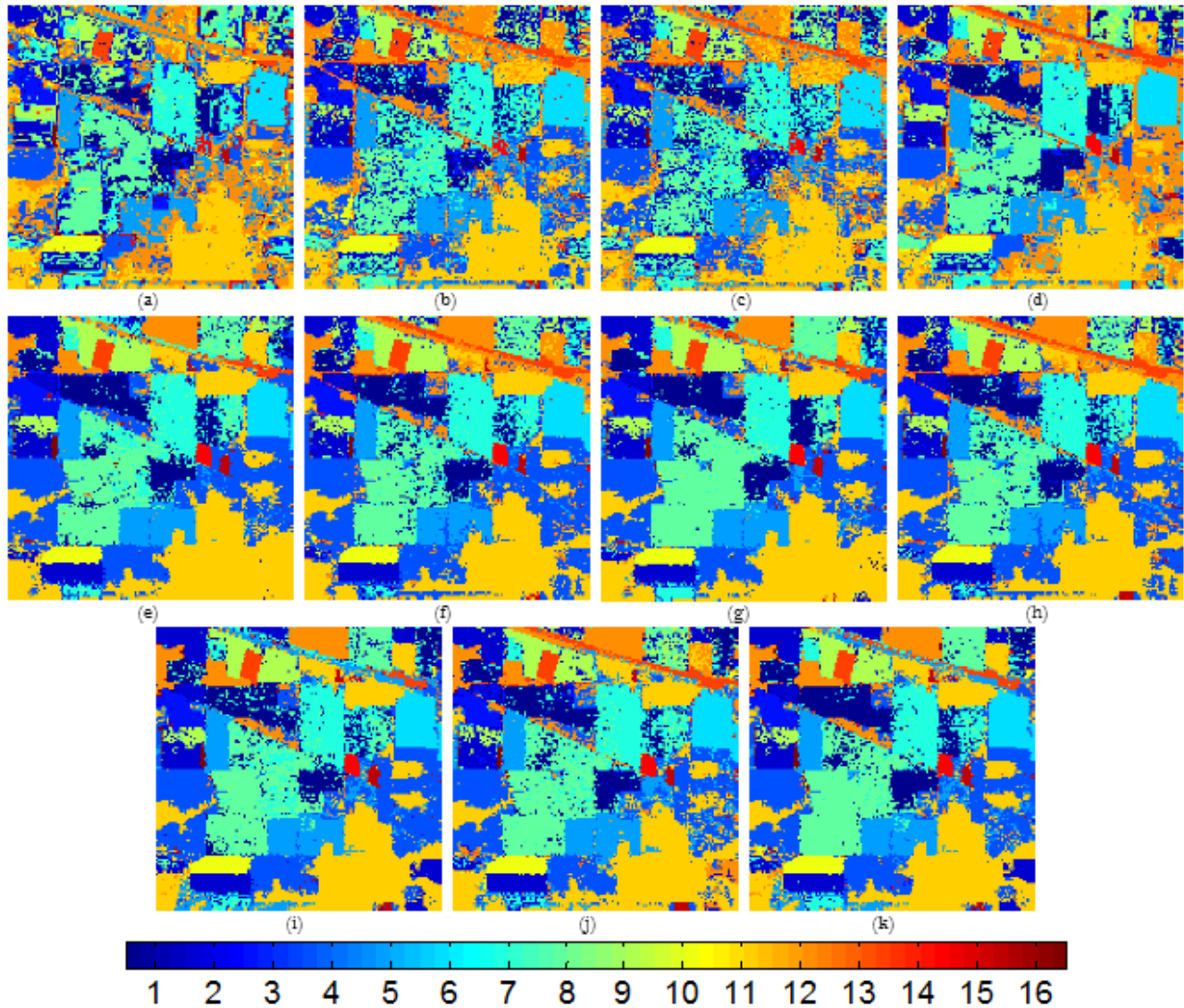


Fig. 5. AVIRIS from (a) to (f), classification maps for different methods after applying DAFE: (a) *Raw*, (b) *AP*, (c) *DA\_DA*, (d) *DA\_DB*, (e)  $\zeta_{DA}$ , (f)  $\zeta_{DB}$ . From (g) to (k) classification maps of different methods after applying DBFE: (g) *AP*, (h) *DB\_DA*, (i) *DB\_DB*, (j)  $\zeta_{DBA}$ , (k)  $\zeta_{DB}$ .

OA of Spectral, *AP*, *DB\_DA*, *DB\_DB*,  $\zeta_{DB}$  by more than 26, 1.7, 6.2, 6.5 and 7.9 in percentage, respectively.

As can be seen from Tables VII and IX, *AP* provides 585 and 720 features, respectively. The table shows that RF can properly handle classification problems consisting of high-dimensional input features and limited training samples, with acceptable CPU processing time. In almost all cases, DAFE outperforms DBFE in terms of classification accuracies and CPU processing time. A possible reason for this may be the fact that the number of selected features used by DBFE is not sufficient. As a result, more features need to be considered in order to provide more consistent results in the case of DBFE, which can be computationally intensive and its performance is highly dependent on the training samples.

#### IV. CONCLUSION

In this paper, we have developed a new automatic framework for the classification of hyperspectral images. Our framework uses both spectral and spatial information. In order to include the spatial information, morphological attribute profiles are taken into account. For reducing the redundancy of the extracted features and deal with the curse of dimensionality introduced by the Hughes effect, supervised feature extraction methods (DAFE and DBFE) are considered. The proposed framework is extensively tested on two widely used hyperspectral data sets, i.e., the ROSIS-03 Pavia University scene and the AVIRIS Indian Pines. Different methods have been used to implement the presented framework, and the results provided have been compared in terms of classification accuracies and CPU processing time.

It should be noted that the two selected hyperspectral data sets represent very different case studies collected by different

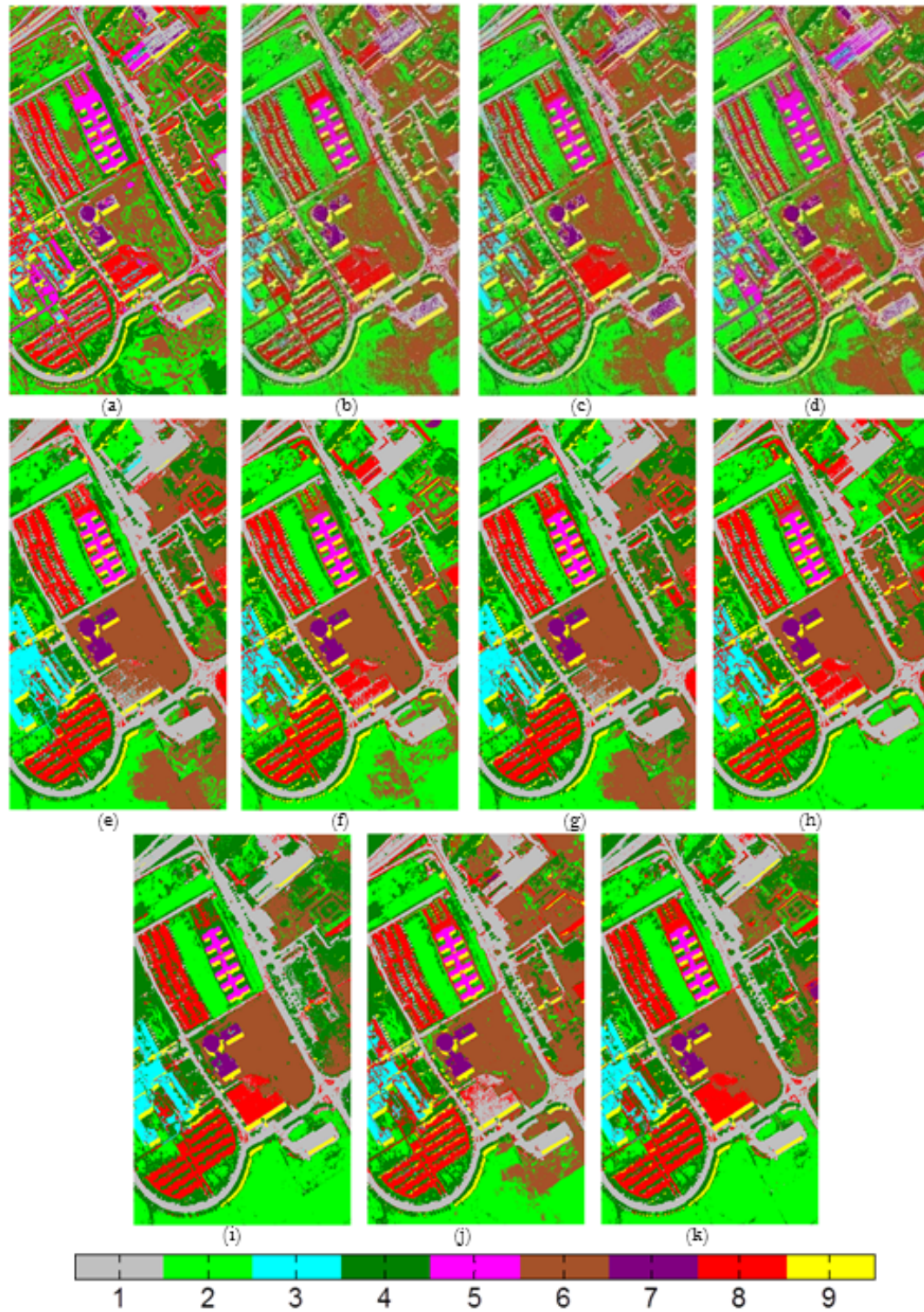


Fig. 6. Pavia University: From (a) to (f), classification maps for different methods started by DAFE: (a) *Raw*, (b) *AP*, (c) *DA\_DA*, (d) *DA\_DB*, (e)  $\zeta_{DA}$ , (f)  $\zeta_{DB}$ . From (g) to (k) classification maps of different methods started by DBFE: (g) *AP*, (h) *DB\_DA*, (i) *DB\_DB*, (j)  $\zeta_{DBA}$ , (k)  $\zeta_{DB}$ .

instruments. The former is related to urban area problems and presents high spatial resolution. In turn, the latter has medium-size spatial resolution and is related to agricultural land-cover classification problems. The good classification accuracies obtained in both case studies indicate the good generalization properties of the presented framework. In addition, the new approach achieves better classification accuracies than other widely used classification techniques, with acceptable CPU processing time. We emphasize that the proposed procedure is fully automatic, which is a highly desirable feature.

A topic of future investigation is the optimal selection (in terms of classification accuracies) of the feature extraction method in the second stage of the proposed approach. Another topic deserving future research is the development of parallel implementations of the presented approach in high performance computing architectures, although the processing times reported in our experiments (measured in a standard desktop CPU) are quite fast for the considered data sets.

## V. ACKNOWLEDGMENT

The ROSIS data and corresponding reference information were kindly provided by from Prof. Paolo Gamba from the University of Pavia, Italy. This work was supported in part by the Icelandic Research Fund for Graduate Students.

## REFERENCES

- [1] A. Plaza, J. A. Benediktsson, J. W. Boardman, J. Brazile, L. Bruzzone, G. Camps-Valls, J. Chanussot, M. Fauvel, P. Gamba, A. Gualtieri, M. Marconcini, J. C. Tilton, and G. Trianni, "Recent advances in techniques for hyperspectral image processing," *Remote Sensing of Environment*, vol. 113, Supplement 1, no. 0, pp. S110 – S122, 2009.
- [2] G. Hughes, "On the mean accuracy of statistical pattern recognizers," *IEEE Trans. Inf. Theory*, vol. IT, no. 14, pp. 55 – 63, 1968.
- [3] D. A. Landgrebe, *Signal Theory Methods in Multispectral Remote Sensing*. Hoboken, NJ: Wiley, 2003.
- [4] P. Ghamisi, M. S. Couceiro, and J. A. Benediktsson, "Classification of hyperspectral images with binary fractional order darwinian pso and random forests," pp. 88 920S–88 920S–8, 2013. [Online]. Available: <http://dx.doi.org/10.1117/12.2027641>
- [5] S. Tadjudin and D. Landgrebe, "Classification of high dimensional data with limited training samples," in *Tech. Rep., School of Electrical and Computer Engineering, Purdue University*, 1998.
- [6] M. Fauvel, Y. Tarabalka, J. A. Benediktsson, J. Chanussot, and J. C. Tilton, "Advances in spectral-spatial classification of hyperspectral images," *Proceedings of the IEEE*, vol. 101, no. 3, pp. 652–675, 2013.
- [7] H. Derin and P. A. Kelly, "Discrete-index Markov-type random processes," *Proceedings of the IEEE*, vol. 77, no. 10, pp. 1485–1510, 1989.
- [8] F. Bovolo and L. Bruzzone, "A context-sensitive technique based on support vector machines for image classification," *Proc. Pattern Recognition and Machine Intelligence*, pp. 260–265, 2005.
- [9] P. Ghamisi, J. A. Benediktsson, and M. O. Ulfarsson, "Spectral-spatial classification of hyperspectral images based on hidden Markov random fields," *IEEE Trans. on Geos. and Remote Sens.*, vol. PP, no. 99, pp. 1–10, 2013. [Online]. Available: <http://dx.doi.org/10.1109/TGRS.2013.2263282>
- [10] P. Ghamisi, M. S. Couceiro, N. M. F. Ferreira, and L. Kumar, "Use of darwinian particle swarm optimization technique for the segmentation of remote sensing images," *Proceedings of the IEEE International Geoscience and Remote Sensing Symposium*, pp. 4295–4298, 2012.
- [11] P. Ghamisi, M. S. Couceiro, J. A. Benediktsson, and N. M. F. Ferreira, "An efficient method for segmentation of images based on fractional calculus and natural selection," *Expert Systems Applications*, vol. 39, no. 16, pp. 12 407–12 417, 2012.
- [12] Y. Tarabalka, J. A. Benediktsson, and J. Chanussot, "Spectral-spatial classification of hyperspectral imagery based on partitional clustering techniques," *IEEE Transactions on Geoscience and Remote Sensing*, vol. 47, no. 5, pp. 2973–2987, 2009.
- [13] P. Ghamisi, M. S. Couceiro, F. M. Martins, and J. A. Benediktsson, "Multilevel image segmentation approach for remote sensing images based on fractional-order darwinian particle swarm optimization," *IEEE Transactions on Geoscience and Remote Sensing*, accepted for publication, vol. PP, no. 99, pp. 1–13, 2013.
- [14] P. Ghamisi, M. S. Couceiro, M. Fauvel, and J. A. Benediktsson, "Integration of segmentation techniques for classification of hyperspectral images," *IEEE Geoscience and Remote Sensing Letters*, accepted for publication, vol. 11, no. 1, pp. 342–346, 2014.
- [15] M. Pesaresi and J. A. Benediktsson, "A new approach for the morphological segmentation of high-resolution satellite imagery," *IEEE Transactions on Geoscience and Remote Sensing*, vol. 39, no. 2, pp. 309–320, 2001.
- [16] J. A. Palmason, J. A. Benediktsson, J. R. Sveinsson, and J. Chanussot, "Classification of hyperspectral data from urban areas using morphological preprocessing and independent component analysis," *Proceedings of the IEEE International Geoscience and Remote Sensing Symposium*, no. 3, p. 176 179, 2005.
- [17] M. Dalla Mura, J. Benediktsson, B. Waske, and L. Bruzzone, "Morphological attribute profiles for the analysis of very high resolution images," *IEEE Transactions on Geoscience and Remote Sensing*, vol. 48, no. 10, pp. 3747–3762, 2010.
- [18] M. Pedernana, P. Marpu, M. Dalla Mura, J. Benediktsson, and L. Bruzzone, "A novel technique for optimal feature selection in attribute profiles based on genetic algorithms," *IEEE Transactions on Geoscience and Remote Sensing*, vol. 51, no. 6, pp. 3514–3528, 2013.
- [19] L. Breiman, "Random forests," *Mach. Learn.*, vol. 45, no. 1, p. 532, 2001.
- [20] —, "RF tools a class of two eyed algorithms," *SIAM Workshop*, 2003.

- [21] P. Marpu, M. Pedergnana, M. Dalla Mura, J. A. Benediktsson, and L. Bruzzone, "Automatic generation of standard deviation attribute profiles for spectral-spatial classification of remote sensing data," *IEEE Geoscience and Remote Sensing Letters*, vol. 10, no. 2, pp. 293–297, 2013.
- [22] C. Lee and D. A. Landgrebe, "Decision boundary feature extraction for non-parametric classification," *IEEE Transactions on System, Man, and Cybernetics*, vol. 23, no. 2, pp. 433–444, 1993.
- [23] K. Fukunaga, *Introduction to Statistical Pattern Recognition*. Academic Press, 1974.
- [24] L. Jimenez and D. A. Landgrebe, "Hyperspectral data analysis and supervised feature reduction via projection pursuit," *IEEE Transactions on Geoscience and Remote Sensing*, vol. 37, no. 6, pp. 2653–2667, 1999.
- [25] C. Lee and D. A. Landgrebe, "Feature extraction based on decision boundaries," *IEEE Transactions on Pattern Analysis and Machine Intelligence*, vol. 15, no. 4, pp. 388–400, 1993.
- [26] J. Serra, *Mathematical Morphology, Theoretical Advances*. New York: Academic Press, 1988, vol. 2.
- [27] —, *Image Analysis and Mathematical Morphology*. Academic Press, 1982.
- [28] P. Soille, *Morphological Image Analysis, Principles and Applications*, Berlin, Germany: Springer Verlag, 2003, vol. 2.
- [29] L. Najman and H. Talbot, *Mathematical Morphology*. Wiley-ISTE, 2010.
- [30] E. J. Breen and R. Jones, "Attribute openings, thinnings, and granulometries," *Computer Vision and Image Understanding*, vol. 64, no. 3, pp. 377 – 389, 1996.
- [31] M. D. Mura, J. A. Benediktsson, B. Waske, and L. Bruzzone, "Morphological attribute filters for the analysis of very high resolution remote sensing images," *Geoscience and Remote Sensing Symposium, 2009 IEEE International, IGARSS 2009*, vol. 3, pp. III–97–III–100, 2009.
- [32] P. Salembier, A. Oliveras, and L. Garrido, "Antiextensive connected operators for image and sequence processing," *IEEE Transactions on Image Processing*, vol. 7, no. 4, pp. 555–570, 1998.
- [33] V. Caselles and P. Monasse, *Geometric Description of Images as Topographic Maps*, 1st ed. Springer Publishing Company, Incorporated, 2009.
- [34] M. H. W. Erik R. Urbach, Jos B.T.M. Roerdink, "Connected shape-size pattern spectra for rotation and scale-invariant classification of gray-scale images," *IEEE Transactions on Pattern Analysis and Machine Intelligence*, vol. 29, pp. 272–285, 2007.
- [35] X. Huang and L. Zhang, "An svm ensemble approach combining spectral, structural, and semantic features for the classification of high-resolution remotely sensed imagery," *IEEE Trans. Geos. Remote sens.*, vol. 51, no. 1, pp. 257–272, 2013.
- [36] M. Dalla Mura, "Advanced techniques based on mathematical morphology for the analysis of remote sensing images," *Ph.D Dissertation, University of Trento, Trento, Italy*, 2011.
- [37] J. A. Richards and X. Jia, *Remote Sensing Digital Image Analysis*, 4th ed. Springer Berlin Heidelberg, 2006.
- [38] P. Ghamisi, J. A. Benediktsson, and J. R. Sveinsson, "Automatic spectral-spatial classification framework based on attribute profiles and supervised feature extraction," *IEEE Trans. Rem. Sens. and Geos.*, In press.
- [39] M. Fauvel, J. A. Benediktsson, J. Chanussot, and J. R. Sveinsson, "Spectral and spatial classification of hyperspectral data using SVMs and morphological profiles," *IEEE Transactions on Geoscience and Remote Sensing*, vol. 46, no. 11, pp. 3804–3814, 2008.
- [40] Y. Tarabalka, M. Fauvel, J. Chanussot, and J. A. Benediktsson, "SVM- and MRF-based method for accurate classification of hyperspectral images," *IEEE Geoscience and Remote Sensing Letters*, 2010.
- [41] M. Dalla Mura, A. Villa, J. A. Benediktsson, J. Chanussot, and L. Bruzzone, "Classification of hyperspectral images by using extended morphological attribute profiles and independent component analysis," *IEEE Geoscience and Remote Sensing Letters*, vol. 8, no. 3, 2011.



**Pedram Ghamisi** graduated with a B.Sc. degree in Civil (Survey) Engineering from the Tehran South Campus of Azad University. Then, he obtained the M.Sc. degree in Remote Sensing at K.N.Toosi University of Technology in 2012. He received the Best Researcher Award for M.Sc. students in K. N. Toosi University of Technology in the academic year 2010-2011. Mr. Ghamisi was the recipient of the IEEE Mikio Takagi Prize which was awarded for the first place in the Student Paper Competition at the 2013 IEEE International Geoscience and Remote Sensing Symposium (IGARSS), Melbourne, July 2013. He is currently a Ph.D. student in Electrical and Computer Engineering at the University of Iceland. His research interests are in remote sensing and image analysis with the current focus on spectral and spatial techniques for hyperspectral image classification. He serves as a reviewer for a number of journals including IEEE Trans. Image Processing, IEEE JSTARS and IEEE GRSL.



**Jón Atli Benediktsson** Jón Atli Benediktsson received the Cand.Sci. degree in electrical engineering from the University of Iceland, Reykjavik, in 1984, and the M.S.E.E. and Ph.D. degrees from Purdue University, West Lafayette, IN, in 1987 and 1990, respectively. He is currently Pro Rector for Academic Affairs and Professor of Electrical and Computer Engineering at the University of Iceland. His research interests are in remote sensing, biomedical analysis of signals, pattern recognition, image processing, and signal processing, and he has

published extensively in those fields. Prof. Benediktsson was the 2011-2012 President of the IEEE Geoscience and Remote Sensing Society (GRSS) and has been on the GRSS AdCom since 2000. He was Editor of the IEEE Transactions on Geoscience and Remote Sensing (TGRS) from 2003 to 2008 and has served as Associate Editor of TGRS since 1999, the IEEE Geoscience and Remote Sensing Letters since 2003 and IEEE Access since 2013. He is on the International Editorial Board of the International Journal of Image and Data Fusion and was the Chairman of the Steering Committee of IEEE Journal of Selected Topics in Applied Earth Observations and Remote Sensing (J-STARS) 2007-2010. Prof. Benediktsson is a co-founder of the biomedical start up company Oxymap ([www.oxymap.com](http://www.oxymap.com)). He is a Fellow of the IEEE and a Fellow of SPIE. He received the Stevan J. Kristof Award from Purdue University in 1991 as outstanding graduate student in remote sensing. In 1997, Dr. Benediktsson was the recipient of the Icelandic Research Council's Outstanding Young Researcher Award, in 2000, he was granted the IEEE Third Millennium Medal, in 2004, he was a co-recipient of the University of Iceland's Technology Innovation Award, in 2006 he received the yearly research award from the Engineering Research Institute of the University of Iceland, and in 2007, he received the Outstanding Service Award from the IEEE Geoscience and Remote Sensing Society. He is co-recipient of the 2012 IEEE Transactions on Geoscience and Remote Sensing Paper Award. He received the 2013 IEEE/VFI Electrical Engineer of the Year Award and in 2013 he was a co-recipient of the IEEE GRSS Highest Impact Paper Award. He is a member of the Association of Chartered Engineers in Iceland (VFI), Societas Scinetiarum Islandica and Tau Beta Pi.



**Antonio Plaza** is an Associate Professor (with accreditation for Full Professor) with the Department of Technology of Computers and Communications, University of Extremadura, where he is the Head of the Hyperspectral Computing Laboratory (Hyper-Comp). He was elevated to IEEE Senior Member status in 2007. He was the Coordinator of the Hyperspectral Imaging Network, a European project with total funding of 2.8 MEuro (2007-2011). He authored more than 370 publications, including more than 100 JCR journal papers (60 in IEEE journals),

20 book chapters, and over 230 peer-reviewed conference proceeding papers (90 in IEEE conferences). He has guest edited seven special issues on JCR journals (three in IEEE journals). He has been a Chair for the IEEE Workshop on Hyperspectral Image and Signal Processing: Evolution in Remote Sensing (2011). He is a recipient of the recognition of Best Reviewers of the IEEE Geoscience and Remote Sensing Letters (in 2009) and a recipient of the recognition of Best Reviewers of the IEEE Transactions on Geoscience and Remote Sensing (in 2010), a journal for which he has served as Associate Editor in 2007-2012. He is also an Associate Editor for the IEEE Geoscience and Remote Sensing Magazine, and was a member of the Editorial Board of the IEEE Geoscience and Remote Sensing Newsletter (2011-2012) and a member of the steering committee of the IEEE Journal of Selected Topics in Applied Earth Observations and Remote Sensing (2012). He served as the Director of Education Activities for the IEEE Geoscience and Remote Sensing Society (GRSS) in 2011-2012, and is currently serving as President of the Spanish Chapter of IEEE GRSS (since November 2012). He is currently serving as the Editor-in-Chief of the IEEE Transactions on Geoscience and Remote Sensing journal (since January 2013). Additional information: <http://www.umbc.edu/rssi/pl/people/aplaza>



**Gabriele Cavallaro** received the B.S. and M.S. degrees in telecommunications engineering from the University of Trento, Trento, Italy, in 2011 and 2013, respectively. He did his Master thesis at the University of Iceland, Reykjavik, Iceland, in remote sensing field on morphological attribute filters based on the Inclusion Tree for the analysis of very high resolution remote sensing images. At the present he is a Ph.D. student at the University of Iceland, Reykjavik, Iceland, and at the University of Extremadura, Cáceres, Spain.